Chinese Physics C (HEP & NP) Vol. 32, No. 9, Sep., 2008

Collective expansion and hadronization in high energy heavy ion collision experiments*

WANG Ya-Ping(王亚平)[1)] ZHOU Dai-Mei(周代梅)[2)] CAI Xu(蔡勖)[3)]

(Institute of Particle Physics, Central China Normal University, Wuhan 430079, China)

Abstract An overview of research status of soft physics in high energy heavy-ion collision experiments and recent experimental results are presented.

Key words quark-gluon plasma, soft physics, collective expansion, hadronization

PACS 25.75.-q

1 Introduction

High energy nucleus-nucleus collisions provide the means of creating nuclear matter in conditions of extreme temperature and density[1]. After the initial collision, particles begin to exchange momentum and the system begins to build up collectivity. Knowing when and how the collectivity is achieved is the first step towards understanding the dynamics in a hot and dense environment. This paper will give an overview on collective expansion of a thermalized system and hadronization in high energy heavy ion collision experiments.

For the collective expansion, we will focus on two areas: radial flow and azimuthal anisotropy. Radial flow is the only possible type of transverse flow allowed by symmetry for central collision. Radial flow can find out when and at which energy density the thermal pressure builds and begins to drive the collective expansion. For azimuthal anisotropy, here three kinds of flow will display: (a) Elliptic flow, which is sensitive to the early stage equation of state. (b) Direct flow, which reflects important features of the system evolution from its initial conditions. (c) Higher harmonics (v_4, v_6, etc.), may be sensitive probes of hydrodynamic behavior and the initial conditions of the collision system.

For the hadronization, we will focus on four parts: hadron spectrum, strangeness enhancement, particle yield and baryon number. Strangeness production, strangeness enhancement and their ratios are important means to understand the baryon production mechanism. There are two kinds of mechanism for baryon production, one is the concept of quark-diquark string breaking, and the other is the concept of string junctions. Measurements of baryon distribution over a large rapidity interval are expected to give answers to different mechanisms of baryon number transport.

An overview of global properties of soft physics, including collision geometry and particle production, has been presented by Y. P. WANG, et al.[2]. Also an overview on correlations and fluctuation has been presented by D. M. Zhou, et al.[3]. Together with this paper, we completely present an review on research status of soft physics in high energy heavy ion collision experiments from SPS to RHIC, and meanwhile we give an outlook for LHC on soft physics. We also suggest readers refer to an overview entitled "experimental status of ultra-high energy induced nuclear reactions" presented by X. CAI[4].

2 Collective expansion

A distinguishing feature of A+A collisions compared to either p-p or p+A collisions is the collective flow observed. This effect is seen over the full range of energies studied in heavy ion collisions, from inci-

Received 22 October 2007

* Supported by Ministry of Education of China (306022) and National Natural Science Foundation of China (10635020)

1) E-mail: wangyp@iopp.ccnu.edu.cn

2) E-mail: zhoudm@phy.ccnu.edu.cn

3) E-mail: xcai@mail.ccnu.edu.cn

714 — 727

dent kinetic energy of 100 AMeV to c.m. energy of $\sqrt{s_{\rm NN}}$=200 GeV[5]. Collective flow is a collective effect which can not be obtained from a superposition of independent N-N collisions.

2.1 Radial flow

Consider a nuclear fireball undergoing collective expansion. Collective flow is defined by the following operational procedure: at any space-time point x in the fireball, they consider an infinitesimal volume element centered at that point and add up all the 4-momenta of the quanta in it. The total 3-momentum P obtained in this way, divided by the associated total energy P^0, defines the average "flow" velocity $v(x)$ of the matter at point x through the relation $P/p^0 = v$. Collective flow thus describes a correlation between the average momentum of the particles with their space-time position, the so-called x-p-correlation. The flow velocity $v(x)$ can be separated into its components along the beam direction ("longitudinal flow" $v_{\rm L}$) and in the plane perpendicular to the beam ("transverse plane") which can be called "transverse flow" $v_\perp$. The magnitude $v_\perp$ may depend on the azimuthal angle around the beam direction. i.e. on the angle between $v_\perp$ and the impact parameter b of the collision. In this case the transverse flow can be called "anisotropic". Its azimuthal average can be called radial flow.

In a hydro-dynamical picture, the $m_{\rm T}$-spectra of particles are sensitive to transverse flow. To characterize the flow, the spectra were fitted with[6]

$$\frac{{\rm d}N}{m_{\rm T}{\rm d}m_{\rm T}{\rm d}y} \propto m_{\rm T} K_1\left(\frac{m_{\rm T}\cosh\rho}{T}\right) I_0\left(\frac{P_{\rm T}\sinh\rho}{T}\right). \tag{1}$$

A combined fit of several spectra with this function allows to determine the thermal freeze-out temperature T and the mean transverse flow velocity $\beta_{\rm T}(\rho = {\rm atanh}\beta_{\rm T})$.

Figure 1 shows such fit to hadronic $m_{\rm T}$-spectra measured by the NA49 Collaboration[7] in Pb+Pb collisions at the SPS at three different beam energies.

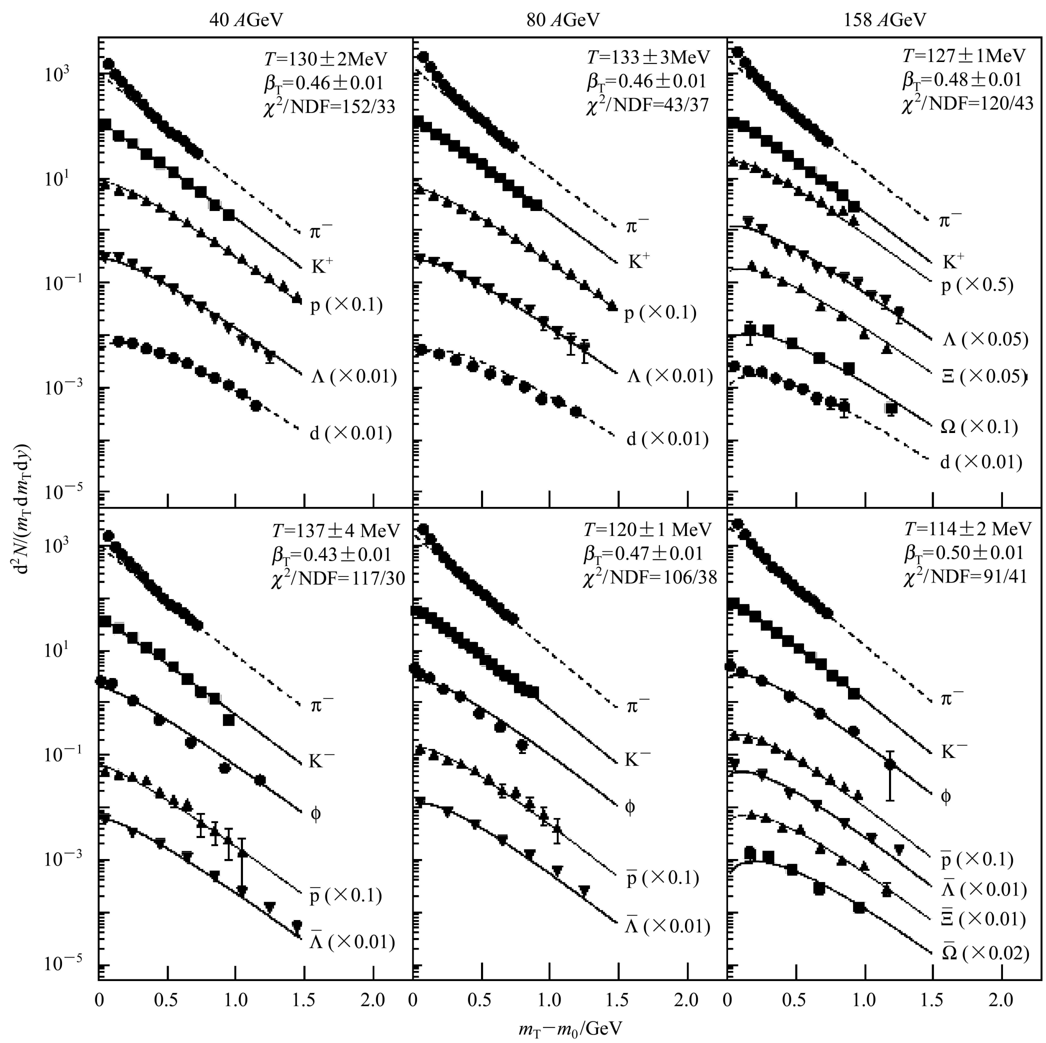

Fig. 1. Positively and negatively charged hadron spectra from Pb+Pb collisions at 40, 80 and 160 AGeV beam energy at the SPS, measured by the NA49 Collaboration. The resulting fit values for T and $\beta_{\rm T}$ are given in the figures.

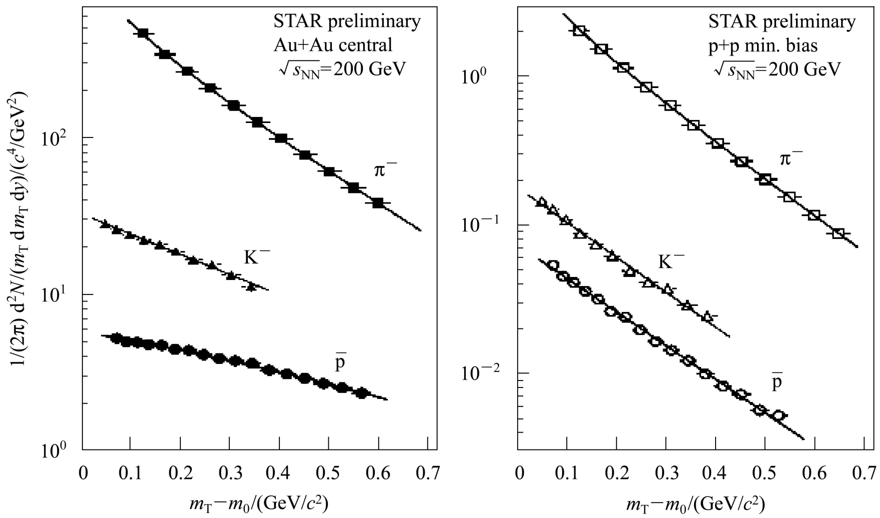

Fig. 2. Pion, kaon and antiproton spectra from 200 AGeV central Au+Au (left) and minimum bias p+p collisions (right), measured by STAR experiment. Note this similar slopes for kaons and antiprotons in p+p collisions and their dramatically different slopes at low transverse kinetic energy in central Au+Au collisions.

The flattening of the spectra at low transverse kinetic energy $m_T - m_0$ by transverse collective flow is even more dramatic at RHIC. Fig. 2 shows a direct comparison of the negative pion, negative kaon and antiproton spectra in central Au+Au and minimum bias proton-proton collisions at the same center of mass energy[8, 9]. Clearly, in p+p collisions the kaon and antiproton spectra have the same slope, indicating the absence of transverse collective flow. That the pion spectra are steeper than both kaons and antiprotons can be attributed to the contribution of resonance decay pions which accumulate at low transverse momenta. However, the pion spectra in Au+Au are obviously flatter in Au+Au than in p+p, and this is even more true for kaons and antiprotons, with a large difference in slope between those last two. Even without a quantitative fit this is a clear manifestation of strong radial flow.

A two-parameter flow fit on RHIC data from 200 AGeV collisions was performed by J. Burward-Hoy[10], see Fig. 3. Here a box-profile for the transverse density $n_i(r_\perp)$ and a linear transverse velocity profile were used where the number β_T given in Fig. 3 is the surface velocity (the average transverse velocity is $\langle v_\perp \rangle = \dfrac{2}{3}\beta_T$). Again in the most central collisions freeze-out temperatures of about 120 MeV and average radial flow velocities $\langle v_\perp \rangle \approx 0.45$ are found.

An interesting aspect of Fig. 3 is the centrality (Scaled by the number of participants, N_{part}) dependence of the fit parameters: The fit was performed over a very wide range of collision centralities, and one observes that more peripheral collisions tend to develop less radial flow and freeze out at higher temperature.

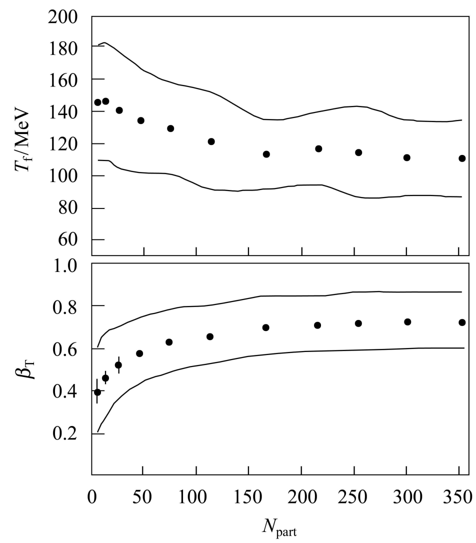

Fig. 3. Kinetic freeze-out temperature T_f and transverse flow velocity β_T at the fireball edge, extracted from a simultaneous fit of a flow spectrum parametrization to $\pi^\pm$, $K^\pm$, p and $\bar{p}$ spectra from 200 AGeV Au+Au collisions over the entire range of centralities. More peripheral collisions are seen to decouple earlier, at higher freeze-out temperature and with less transverse flow.

2.2 Azimuthal anisotropy

For central collisions ($b=0$) between equal spherical nuclei, radial flow is the only possible type of transverse flow allowed by symmetry. In non-central ($b \neq 0$), immediately after an A+A collision, the overlap region defined by the nuclear geometry is the almond shape (see Fig. 4) with the shortest axis along the impact parameter vector. Due to the reaction plane breaking the ϕ symmetry of the problem, the semi-inclusive single particle spectrum is an expansion in harmonics[11] of the azimuthal angle of the particle with respect to the reaction plane, $\phi-\Phi_{\rm R}$[12], as Eq. (2) show. In the Eq.(2), the angle of the reaction plane $\Phi_{\rm R}$ is defined to be along the impact parameter vector, the x axis in Fig. 4.

$$E\frac{\mathrm{d}^3N}{\mathrm{d}^3P}=\frac{1}{2\pi}\frac{\mathrm{d}^2N}{P_{\rm T}\mathrm{d}P_{\rm T}\mathrm{d}y}\left(1+2\sum_{n=1}^{\infty}v_n(p_{\rm t},y)\cos(\phi-\Phi_{\rm R})\right). \tag{2}$$

The expansion parameter v_1 is called the directed flow, v_2 the elliptical flow and higher order anisotropy parameters (v_4, v_6, etc.)[1].

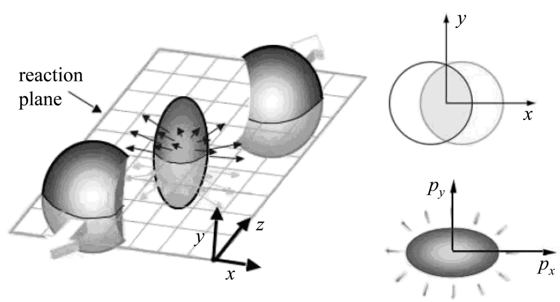

Fig. 4. Left: Almond shaped overlap zone generated just after A+A collision where the incident nuclei are moving along the $\pm z$ axis, and the reaction plane, which by definition contains the impact parameter vector. Right: View of the collision down the z axis: (top) spatial distribution (bottom) momentum distribution after elliptic flow (v_2) develops.

2.2.1 Elliptic flow

The spatial anisotropy turns into an momentum anisotropy only if the outgoing particles (or partons) interact with each other. Thus the momentum anisotropy is proportional to the spatial anisotropy of the almond, represented by the eccentricity, $\varepsilon=(R_y^2-R_x^2)/(R_y^2+R_x^2)\approx(R_y-R_x)/(R_y+R_x)$, at the time ($t_0$) of thermalization. This is due to the fact that the mean number of scatterings in the transverse plane is different along the x and y axes[12—14]. The mean number of scatterings is proportional to the particle density, $\rho=(1/\pi R_xR_y)\mathrm{d}n/\mathrm{d}y$ times the interaction cross section (σ) times the distance traversed:

$$v_2\propto R_y\sigma\frac{1}{\pi R_xR_y}\frac{\mathrm{d}n}{\mathrm{d}y}-R_x\sigma\frac{1}{\pi R_xR_y}\frac{\mathrm{d}n}{\mathrm{d}y}\propto\varepsilon\sigma\frac{1}{\pi R_xR_y}\frac{\mathrm{d}n}{\mathrm{d}y}, \tag{3}$$

where

$$R_x=\sqrt{\langle x^2\rangle},\quad R_y=\sqrt{\langle y^2\rangle}.$$

Since the eccentricity ε is much larger for peripheral than for central collisions, the dependence of v_2 on centrality exhibited a characteristic shape (see Fig. 5(Top))[15]. This is one of the first publications from RHIC and shows that v_2 is surprisingly large and near the hydro-limits. The hydro-limits indicated are for full thermalization of the system at the value of ε given by the initial nuclear geometry of the almond at the time of overlap.

Figure 5 Bottom[16, 17] shows that the v_2 follows the hydro prediction out to $p_{\rm T}\approx 2$ GeV/c and then plateaus at a constant value to much higher $p_{\rm T}$. This is one of the principal arguments for the "perfect fluid" because any modest value of viscosity[18] would cause the v_2 to decrease towards zero near $p_{\rm T}\approx 1.7$ GeV/c (see Fig. 6).

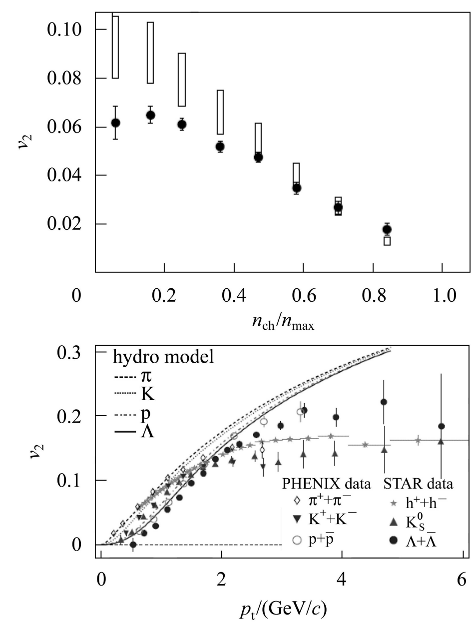

Fig. 5. Top: v_2 as a function of centrality[15]. The boxes represent the expected hydro-limit with $v_2/\varepsilon=0.19$ (lower edge) and 0.25 (upper edge). Bottom: v_2 as a function of $p_{\rm T}$ for the identified particles in minimum bias Au+Au collisions at $\sqrt{s_{\rm NN}}=200$ GeV together with a hydro calculation[16].

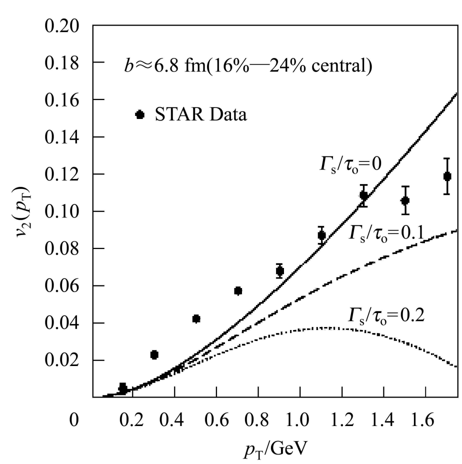

Fig. 6. v_2 as a function of $p_{\rm T}$ in a hydro calculation[18] for mid-central collisions for different values of $\Gamma_{\rm s}/\tau_0$, the "sound attenuation length" which is zero for a "perfect fluid" and increases linearly with the viscosity.

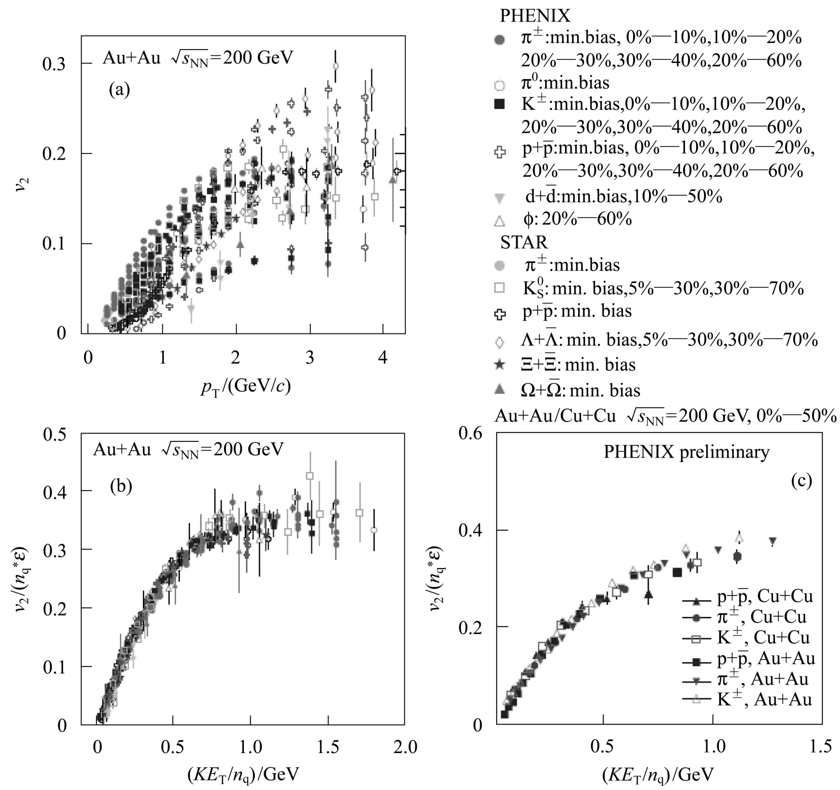

Fig. 7. (a) v_2 vs. p_{T} and (b) $v_2/(n_{\mathrm{q}}\epsilon)$ vs. $KE_{\mathrm{T}}/n_{\mathrm{q}}$ for several centralities and particle species as indicted. (c) $v_2/(n_{\mathrm{q}}\epsilon)$ vs. $KE_{\mathrm{T}}/n_{\mathrm{q}}$ for $\pi^{\pm}$, $\mathrm{K}^{\pm}$, and $(\bar{\mathrm{p}},\mathrm{p})$ from Cu+Cu and Au+Au collisions at $\sqrt{s_{\mathrm{NN}}}=200$ GeV.

Universal scaling of elliptic flow (v_2) has been recently observed at RHIC[19—21]. That is, for a broad range of particle species, v_2/n_{q} vs. $KE_{\mathrm{T}}/n_{\mathrm{q}}$ scales to a single function; here, n_{q} and KE_{T} are the number of valence quarks ($n_{\mathrm{q}}=2,3$ for mesons and baryons respectively) and the transverse kinetic energy of the particle. This observation has been interpreted as evidence that transverse expansion of the matter produced in energetic RHIC collisions, occurs during a phase dominated by partonic collectivity. Fig. 7(a) shows differential flow measurement $v_2(p_{\mathrm{T}})$, for several particle species produced at mid-rapidity in central and semi-central Au+Au collisions at $\sqrt{s_{\mathrm{NN}}}=200$ GeV; they span essentially the full range of measurements at RHIC. Fig. 7(b) shows the scaled results ($v_2/(n_{\mathrm{q}}\epsilon)$ vs. $KE_{\mathrm{T}}/n_{\mathrm{q}}$) obtained from the same data; here ϵ is the integral v_2 of charged hadrons for each of the indicated centrality selections, multiplied by a constant factor $k\approx 3.2$ (i.e. $\epsilon=k\times v_2$)[19—21]. Recent measurements[19] indicate that $v_2(p_{\mathrm{T}})/\epsilon$ is independent of centrality and the size of the colliding system as would be expected from a hydrodynamic system. Fig. 7(b) indicates that the relatively complicated dependence of v_2 on centrality, transverse momentum, particle type, etc., for particles produced at mid-rapidity can be scaled to a single function. Fig. 7(c) demonstrates that the same scaling also holds for $\pi^{\pm}$, ($\mathrm{K}^{\pm}$) and $(\bar{\mathrm{p}},\mathrm{p})$ produced

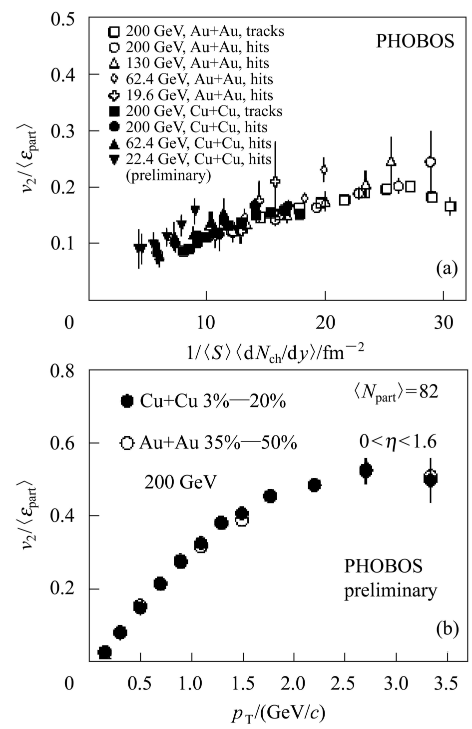

Fig. 8. (a) shows $v_2/\langle\epsilon_{\mathrm{part}}\rangle$ as a function of mid-rapidity ($|\eta|<1$) particles area density $1/\langle S\rangle\langle \mathrm{d}N/\mathrm{d}y\rangle$ for Cu+Cu and Au+Au collisions. (b) $v_2/\langle\epsilon_{\mathrm{part}}\rangle$ as a function of p_{T} for Cu+Cu and Au+Au collisions at 200 GeV with the same area density (same $\langle N_{\mathrm{part}}\rangle=82$).

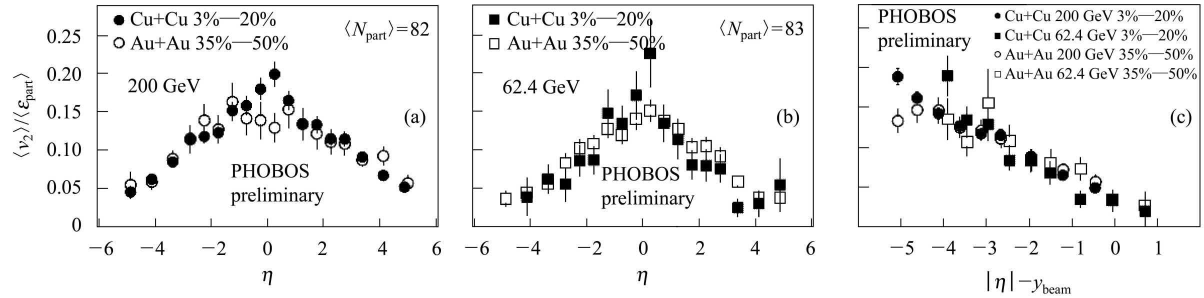

Fig. 9. (a) and (b) show the $v_2/\langle\epsilon_{\rm part}\rangle$ as a function of η for Au+Au (Cu+Cu) collisions with same $\langle N_{\rm part}\rangle$ at 200 and 62.4 GeV, respectively. (c) shows $v_2/\langle\epsilon_{\rm part}\rangle$ as a function of $\eta'=|\eta|-y_{\rm beam}$ for Cu+Cu and Au+Au collisions.

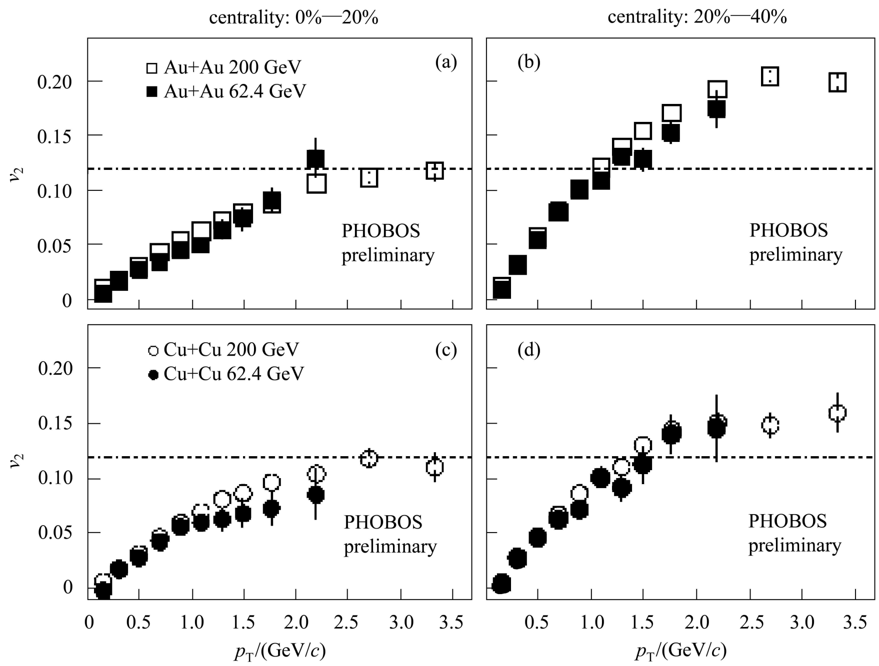

Fig. 10. v_2 vs. $p_{\rm T}$ for Au+Au and Cu+Cu collisions at $\sqrt{s_{\rm NN}}=62.4$ and 200 GeV.

at mid-rapidity in Cu+Cu collisions at $\sqrt{s_{\rm NN}}$ = 200 GeV[22].

Recently PHOBOS Collaboration has given a systematic study of elliptic flow as a function of centrality, pseudorapidity, transverse momentum and energy for Cu+Cu and Au+Au collisions[23]. Elliptic flow scaled by participant eccentricity is found to be similar for both systems when collisions with the same number of participants or the same averages area density are compared, see Fig. 8.

This similarity is also observed over a wide range in pseudorapidity (see Fig. 9)and transverse momentum (see Fig. 10), indicating that participant eccentricity is the relevant quantity for generating the azimuthal asymmetry leading to the observed elliptic flow.

2.2.2 Direct flow

Directed flow, v_1, was discovered almost 23 years ago[24] and has been extensively studied and reviewed at lower beam energies. At RHIC energies directed flow in the central rapidity region reflects important features of the system evolution from its initial conditions. v_1 is predicted to be small near midrapidity with almost no dependence on pseudorapidity. However, it could exhibit a characteristic "wiggle"[25], depending on the baryon stopping and production mechanisms as well as strong space-momentum correlations in the system's evolution. A similar rapidity dependence of direct flow could develop due to a change in the matter compressibility if a quark-gluon plasma is formed[26, 27]. It results in the so-called third flow component[26] or "antiflow"[27] component in the expansion of the matter. This expansion direction is opposite the normal directed flow.

STAR Collaboration presented the results[28] in comparison with the lower beam energy data at the SPS of NA49[29]. The NA49 data were also replotted so as to be at the same distance from beam rapidity as the STAR results (see Fig. 11).

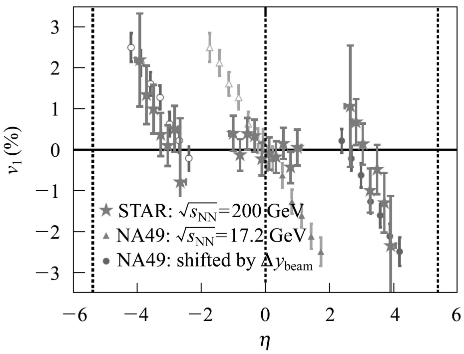

Fig. 11. The values of v_1 (stars) for charged particles for 10% to 70% centrality plotted as a function of pseudorapidity. Also shown are the results from NA49(triangles) for pions from 158 GeV Pb+Pb mid-central (12.5% to 33.5%) collisions plotted as a function of rapidity. The open points have been reflected about midrapidity. The NA49 points have also been shifted (circles) plus or minus by the difference in the beam rapidities of the two accelerators. The dashed lines indicated midrapidity and RHIC beam rapidity.

The RHIC $v_1(\eta)$ resulted differ greatly from the unshifted SPS data in Fig. 11 that they are flat near midrapidity and become significant only at the highest rapidities measured. However, when plotted in the projectile frame relative to their respective beam rapidities, they look similar.

2.2.3 Higher harmonics

Higher order anisotropy parameters (v_4,v_6, etc.) may be very sensitive probes of hydrodynamic behavior and the initial conditions of the collision system[30]. The authors of Ref. [31] argue that values of the ratio v_4/v_2^2 larger than 0.5 indicate deviations from ideal fluid behavior. When measured for identified particles, higher harmonics can also test quark-number scaling[32]. v_4 and v_6 for charged hadrons at 200 GeV are shown in Fig. 12[28]. The STAR Collaboration measured v_4 as a function of p_t, η, and centrality. They observed that v_4 appears to scale approximately as v_2^2, as a function of p_t, η, and centrality. v_6, although essentially zero, is not inconsistent with scaling as v_2^3. This was the first measurement of higher harmonics at RHIC, and it was expected that these higher harmonics would be a sensitive test of the initial configuration of the system, since they provide a Fourier analysis of the shape in momentum space which can be related back to the initial shape in configuration space.

In Fig. 13, the STAR Collaboration plotted pion, kaon, anti-proton and $\Lambda+\bar{\Lambda}$ v_4 for $\sqrt{s_{NN}}$ = 62.4 GeV[33], where the standard event plane method has been used. In the bottom panels of Fig. 13 they show the ratio v_4/v_2^2 for charged pions, neutral kaons, and hyperons. The uncertainty in v_4/v_2^2 from possible non-flow leads to asymmetric errors. The ratio v_4/v_2^2 is well above 0.5 even when errors are taken into account.

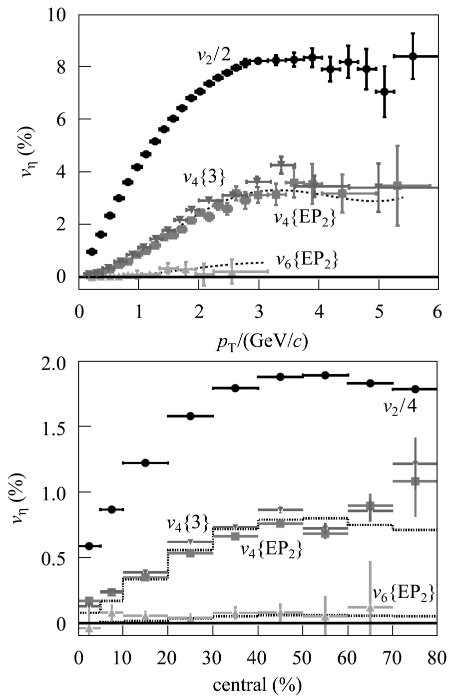

Fig. 12. Top panel: The minimum bias values of v_2, v_4, and v_6 with respect to the second harmonic event plane as a function of p_t for $|\eta|<1.2$. The v_2 values have been divided by a factor of 2 to fit on scale. Also shown are the three particle cumulantive values (triangles) for v_4 ($v_4\{3\}$). The dashed curves are $1.2v_2^2$ and $1.2v_2^3$. Bottom panel: The p_t- and η-integrated values of v_2, v_4, and v_6 as a function of centrality. the v_2 values have been divided by a factor of 4 to fit on scale. Also shown are the three particle cumulantive values for v_4($v_4\{3\}$). The dotted histograms are $1.4v_2^2$ and $1.4v_2^3$.

3 Hadronization

3.1 Hadron spectrum

At RHIC 99.9% of all charged particles have momenta below 2 GeV/c, far outside the range of perturbative QCD[34]. Hadron spectra reflect conditions late in the reaction, as well as the integrated effects of expansion from the beginning of the collision. The hadronic spectra are measured by the NA49 Collaboration[35] in Pb+Pb collisions at the SPS at three different beam energies, see reference[36]. The flattening of the spectra at low transverse kinetic energy $m_\perp - m_0$ by transverse collective flow is even more dramatic at RHIC.

Transverse momentum spectra of identified particles reflect the system at kinetic freeze-out and allow us to extract information from the latest stage of the evolution when the system is still thermally coupled and governed by elastic interactions among its constituents. Fig. 14 shows a compilation of p_T spectra for π^-, K^- and $\bar{p}$ from all four RHIC experiments at $\sqrt{s_{NN}}$=200 GeV[34].

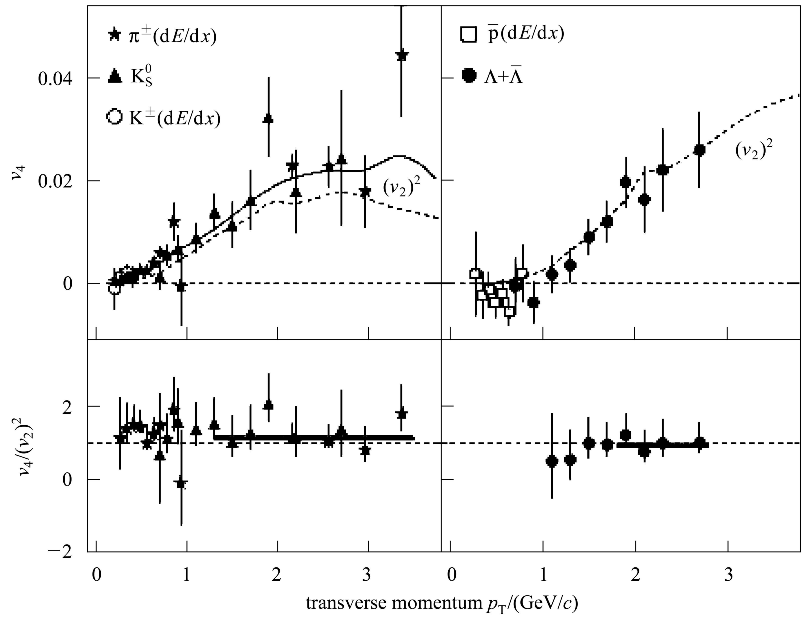

Fig. 13. Top panels: minimum bias v_4 for pions, charged kaons, K_S^0, anti-protons and $\Lambda+\bar{\Lambda}$ at $\sqrt{s_{NN}}$ = 62.4 GeV. In the left panel the solid (dashed) line shows the value for v_2^2 for pions (kaons). Bottom panels: v_4 scaled by v_2^2. The systematic errors on the v_4/v_2^2 ratio from non-flow are included in the error bars leading to asymmetric errors.

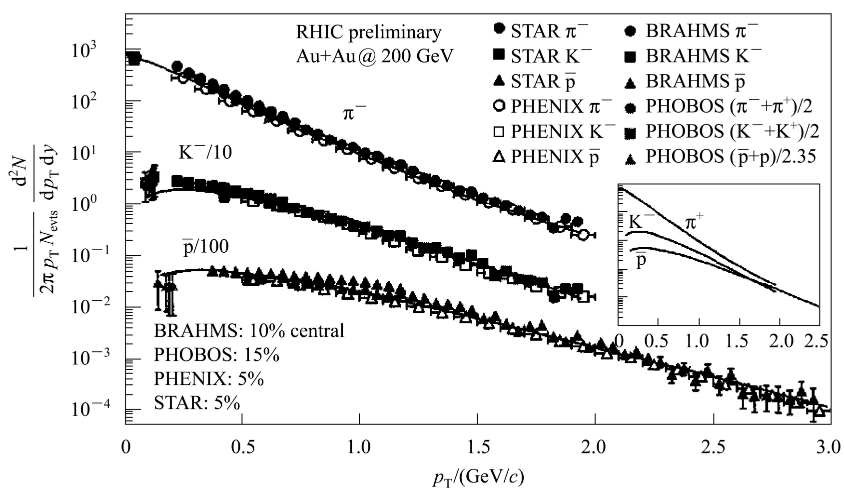

Fig. 14. Compilation of preliminary transverse momentum spectra of π^-, K^- and $\bar{p}$.

The top left panel of Fig. 15 shows the hydrodynamic fit to the transverse momentum spectra of positive pions and antiprotons, as measured by the PHENIX and STAR collaborations in central ($b=0$) Au+Au collisions at $\sqrt{s}$=130 AGeV. The fit yields an initial central entropy density s_{eq}=95 fm^{-3} at an equilibration time τ_{eq}=0.6 fm. This corresponds to an initial temperature of T_{eq}=340 MeV and an initial energy density ϵ=25 GeV/fm^3 in the fireball center. The remaining three panels of Fig. 15 show the transverse momentum spectra of pions, kaons and antiprotons in five different centrality bins as observed by the PHENIX and STAR collaborations. For all centrality classes, except the most peripheral one, the hydrodynamic predictions (solid lines) agree pretty well with the data. The kaon spectra are reproduced almost perfectly, but for pions the model consistently underpredicts the data at low $p_\perp$. This has now been understood to be largely an artifact of having employed in these calculations a chemical equilibrium equation of state all the way down to kinetic freeze-out.

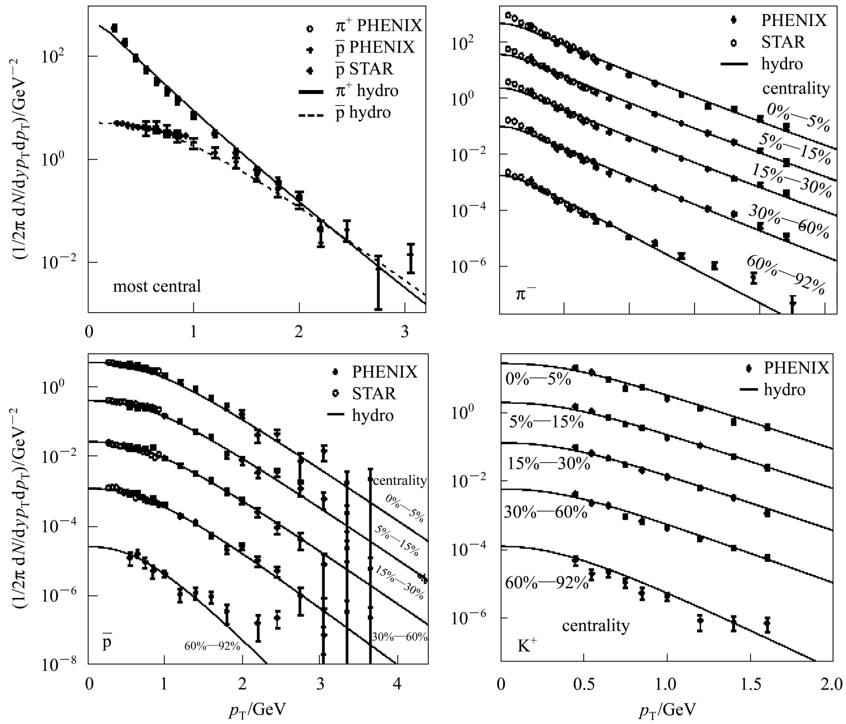

Fig. 15. Identified pion, antiproton and kaon spectra[36] for $\sqrt{s_{NN}}$=130 GeV from the PHENIX and STAR collaborations in comparison with the results from a hydrodynamic calculation.

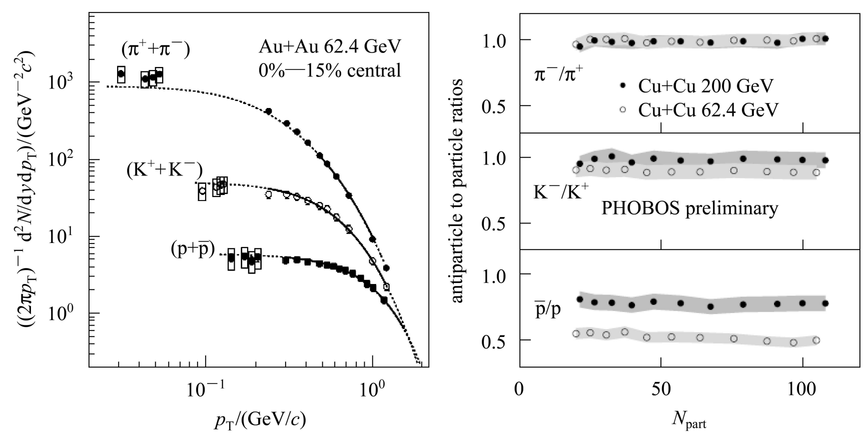

Fig. 16. Left: Identified particle spectra for Au+Au collisions at $\sqrt{s_{NN}}$ = 62.4 GeV. Right: Antiparticle to particle ratios for protons, kaons and pions in Cu+Cu collisions at $\sqrt{s_{NN}}$ = 62.4 and 200 GeV.

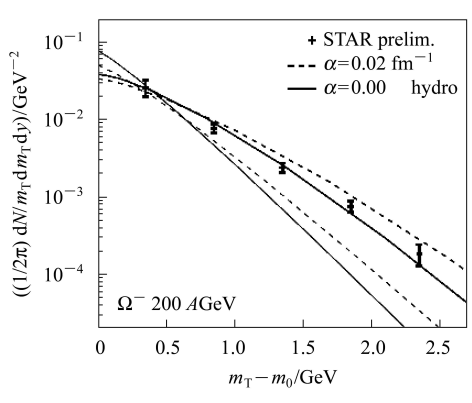

Fig. 17. Transverse mass spectrum of Ω hyperons from central 200 AGeV Au+Au collisions at RHIC[38].

The left panel of Fig. 16 shows identified hadron transverse momentum spectra in Au+Au collisions at very low p_T range[37]. The right panel of the figure shows the ratio of antiparticle to particle as a function of centrality in Cu+Cu collisions, and it's evident that the ratios are weakly dependent on centralities. Meanwhile, we can see that the energy dependence of the proton and kaon particle ratios between $\sqrt{s_{NN}}$=62.4 and 200 GeV is clearly evident except for pions.

Figure 17 compares the preliminary spectra of Ω hyperons[38] with the hydrodynamic predictions[39, 40].

As shown in the Fig. 17, the data clearly favor the flatter curve, suggesting intense rescattering of the Ω's in the hadronic phase. The microscopic mechanism for this rescattering is still unclear. However, without hadronic rescattering the hydrodynamic model, in spite of its perfect local thermalization during the early expansion stages, is unable to generate enough transverse flow to flatten the Ω spectra as much as required by the data.

3.2 Strangeness enhancement

Strange particles produced in heavy ion collisions give important information on the collision mechanism. In particular, the enhanced relative yield of strange and multi-strange particles in nucleus-nucleus reactions with respect to proton-nucleus interactions has been suggested as one of the sensitive signatures for a phase transition to a QGP state[41]. It is expected that the enhancement should be more pronounced for multi-strange than for singly strange particles.

The yields in Pb+Pb interactions are presented as a function of the collision centrality and compared with those obtained from p+Pb collisions. Strangeness enhancement is observed which increases with centrality and with the strangeness content of the hyperon[42]. Λ, Ξ and Ω yields and transverse mass spectra have been measured at central rapidity in Pb+Pb and p+Pb collisions at 158 AGeV/c at SPS. Enhancement of central Λ, Ξ and Ω yields in Pb+Pb collisions at 158 AGeV/c is shown in Fig. 18.

Figure 18(a) shows the Λ, Ξ and Ω yields per event for p+Pb and Pb+Pb interactions as a function of the number of participants. Fig. 18(b) shows the hyperon yields expressed in units of the corresponding yield per p+Pb interaction (i.e. each yield is rescaled so that the value for p+Pb is set to one). All Pb+Pb hyperon yields show a steady increase with centrality up to very central events. The hyperon yields in Pb+Pb are compared to a yield curve (full line) proportional to the number of participants $\langle N_{\rm part}\rangle$ drawn through the p+Pb point in Fig. 18(b). It is observed that the Λ, Ξ and Ω yields increase with centrality

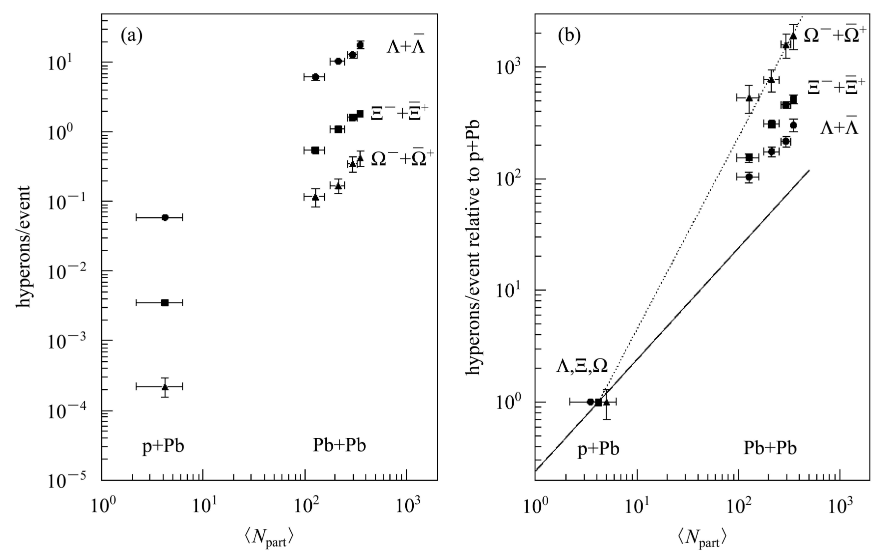

Fig. 18. (a) The Λ, Ξ and Ω yields expressed in units of yields per event. (b) The Λ, Ξ and Ω yields expressed in units of yields observed in p+Pb collisions and compared to yield curves proportional to the $\langle N_{\rm part}\rangle$ (solid curve) and to $\langle N_{\rm part}\rangle^{1.72}$ (dotted curve).

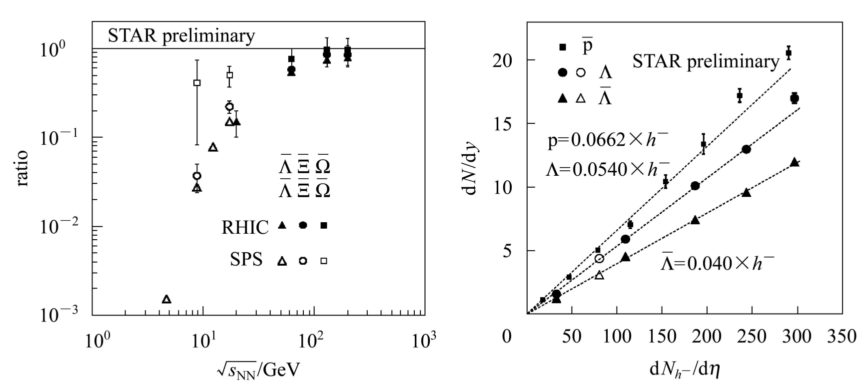

Fig. 19. Left: Strange anti-baryon to baryon ratios as a function of collision energy. Right: dN/dy of $\bar{\rm p}$, Λ and $\bar{\Lambda}$ as a function of h^-.

from p+Pb to Pb+Pb interactions faster than the number of participants, and the enhancements exhibit a marked $\Omega > \Xi > \Lambda$ hierarchy.

The left panel of Fig. 19 shows the ratios of the strange anti-baryon/baryon yields as a function of energy in heavy-ion collisions[43]. The ratios also exhibit an ordering with strangeness content (where $\bar{\Omega}/\Omega > \bar{\Xi}/\Xi > \bar{\Lambda}/\Lambda$). The right panel of Fig. 19 shows that $\mathrm{d}N/\mathrm{d}y$ of $\bar{\mathrm{p}}$, Λ and $\bar{\Lambda}$ have a linear dependence on the pseudorapidity distribution of negative charged particles[44].

Figure 20 shows the enhancement of strange baryons and anti-baryons as a function of centrality as measured by STAR for Au+Au collisions at $\sqrt{s_{\rm NN}} = 200$ GeV[43] and by NA57 for Pb+Pb collisions at $\sqrt{s_{\rm NN}} = 17.3$ GeV[45]. The enhancement is also the same for lower energy SPS data which is in contradiction to the energy dependence which was predicted[46].

3.3 Particle yield

A detailed study of chemical freeze-out in nucleus-nucleus collisions at beam energies of 11.6, 30, 40, 80 and 158 AGeV has been presented by F. Becattini[47]. By analyzing hadronic multiplicities within the statistical hadronization approach, they have studied the strangeness production as a function of centre of mass energy and of the parameters of the source. they show that, in this energy range, the use of hadron yields at midrapidity instead of in full phase space artificially enhances strangeness production and could lead to incorrect conclusions as far as the occurrence of full chemical equilibrium is concerned. As shown in Fig. 21.

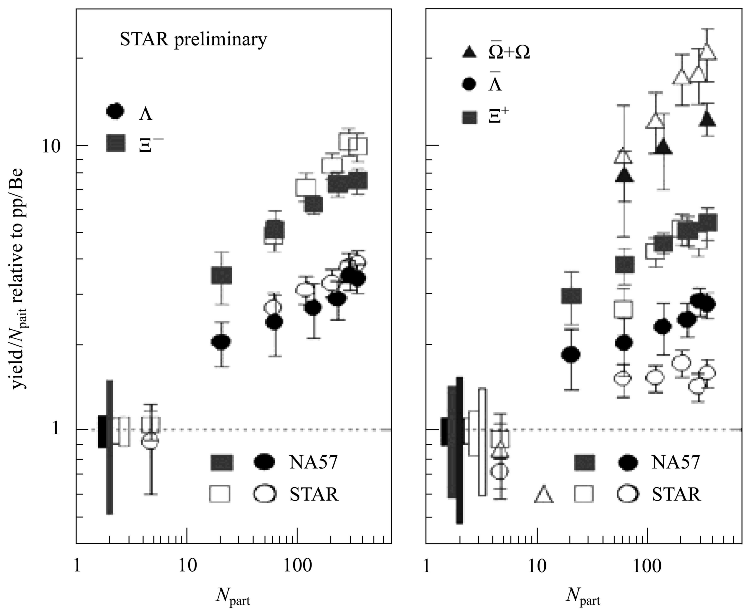

Fig. 20. Enhancement factors versus $N_{\rm part}$ for A+A collisions relative to p-p (STAR) and p+Be (NA57) collisions respectively.

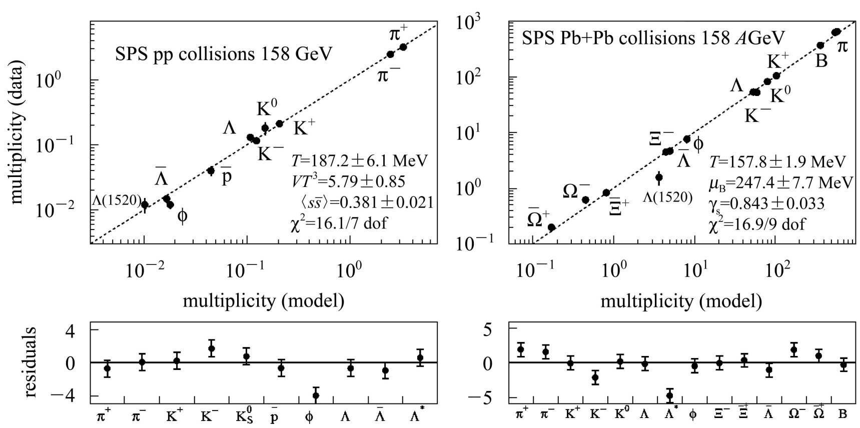

Fig. 21. Left: Above) The measured versus the fitted multiplicities in the statistical model supplemented with strangeness suppression in p-p collisions at a beam energy of 158 GeV corresponding to $\sqrt{s} = 17.2$ GeV; also quoted the best-fit parameters. Below) The residual distribution. Right: The same as the left panel, but in Pb+Pb collisions at a beam energy of 158 AGeV.

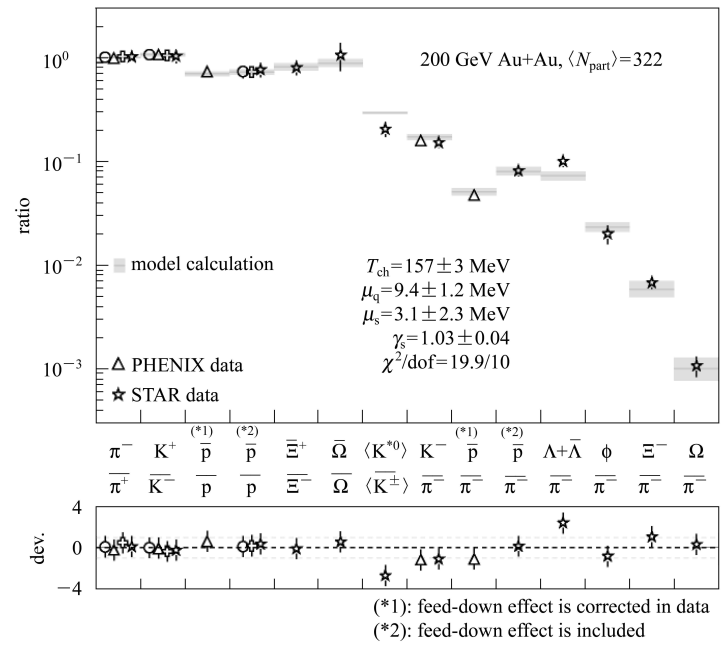

Fig. 22. Comparison of PHENIX (triangles), STAR (stars), BRAHMS (circles), and PHOBOS (crosses) particle ratios from central Au+Au collisions.

In Refs. [48, 49] authors compares the STAR measurements of integrated hadron yield ratios for central Au+Au collisions with statistical model fits. In comparison with results from p-p collisions at similar energies, the relative yield of multi-strange baryons Ξ and Ω is considerably enhanced in RHIC Au+Au collisions. And non-equilibrium parameter γ_s rises from $\approx$0.7 in the peripheral Au+Au collisions to values statistically consistent with unity for central collisions.

Figure 22 shows the comparison of the thermal model results with the RHIC experimental data.

One sees in Fig. 22 that the overall agreement is very good. Most of the data are reproduced by the model within the experimental errors.

Through the above figures, we have shown that the statistical model in complete equilibrium gives results consistent with the experimental data for particle production in Au+Au collisions at $\sqrt{s_{NN}} = 200$ GeV. At this energy the chemical freeze-out appears at T_{ch}=157±3 MeV and μ_B=23±3 MeV, and γ_s=1.03±0.04. In contrast to the controversies at lower beam energies, the observation that strangeness is equilibrated is common to all thermal calculations that reproduce the RHIC data[50].

3.4 Baryon number

The phase transformation at a vanishing baryon density has been ascertained to be continuous. As a result, one would expect that the various conserved quantities such as the baryon number, charge and strangeness remain more or less unchanged within various sub-volumes of the phase space occupied by the system[51]. Baryon number is a locally conserved quantity, and thus its distribution is not easily influenced by final state interactions. The net baryon number in nucleons is carried by the valence quarks.

The conserved net-baryon number is established from the incoming nuclei, but becomes spread over the rapidity interval by initial interactions, and then additionally smeared by the rescattering process; together these make up transport of baryon number from the nuclei to their final rapidities[52]. Fig. 23 shows a characterization of the baryon-antibaryon differences as a function of strange quart content $|s|$.

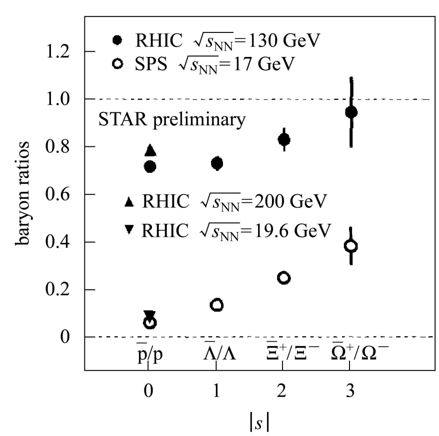

Fig. 23. Mid-rapidity antibaryon to baryon ratios are shown for various species and at several energies of central heavy ion collisions.

It's clear from the plot that the ratios tend towards one with increasing strangeness content and with increasing energy. The ratios also indicate that the yield of baryons resulting from pair production processes has begun to dominate over those from transport at RHIC energies. STAR has also measured most of these antibaryon to baryon ratios as a function of centrality and sees only slight rise in the antiproton to proton ratio for peripheral collisions, and no significant changes for the other ratios[53].

Net baryons from these collisions continue to decrease with increasing energy, but are still nonzero, as shown in Fig. 24.

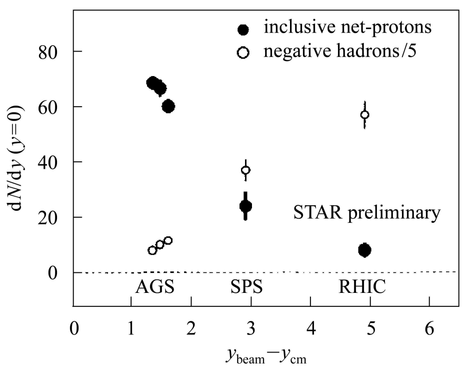

Fig. 24. The net protons at mid-rapidity versus collision energy for central collisions.

The plot means that pair production processes behind baryon yields are now dominant, but do not account for all baryon number; there must remain some transport of baryon number even over ∼5 and ∼6 units of rapidity at 130 and 200 GeV respectively.

Figure 25 shows the integrated yields, $dN/d\eta$, of net protons in mid-rapidity range at 62.4 and 200 GeV energies[54].

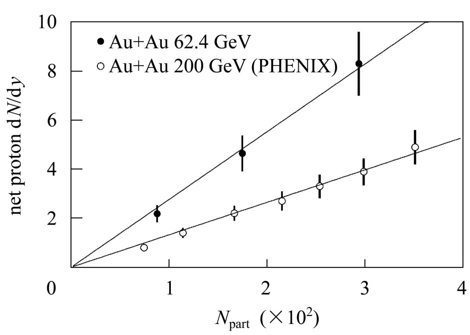

Fig. 25. Net-proton yield close to mid-rapidity as a function of $N_{\rm part}$ in Au+Au collisions at $\sqrt{s_{\rm NN}}$ = 62.4 and 200 GeV.

The net proton yield is approximately proportional to $N_{\rm part}$, which does not meet the expectations of increasing amount of baryon stopping with increasing centrality. According to Fig. 16, the $\bar{\rm p}/{\rm p}$ ratio is not dependent on centrality, so the yields of $\bar{\rm p}$ and p are all proportional to the $N_{\rm part}$.

4 Conclusion

After the overview of research status of soft physics on collective expansion and hadronization in high energy heavy ion collision experiments, we try to give a conclusion as follows:

(1) Results from RHIC supply evidence for a hydrodynamic expansion of a thermalized system, in which the collectivity is achieved fast and at the very early time. Understanding the initial condition plays a key role in understanding what happens thereafter. Studying elliptic flow fluctuation, as well as directed flow for high $p_{\rm T}$ particles, may help us constraint the initial condition.

(2) $dN_{\rm ch}/d\eta$ and strangeness enhancement have been observed in heavy ion collisions at lower energies, and they change smoothly as a function of $\sqrt{s_{\rm NN}}$ from AGS to SPS to RHIC. The yields of different hadron species are proportional to the $N_{\rm part}$. Meanwhile, these yields up to and including multi-strange hadrons, become consistent with a grand canonical statistical distribution at a chemical freeze-out temperature $T_{\rm ch}$ and a baryon chemical potential $\mu_{\rm B}$. The ratio of final state hadrons can be described by the temperature $T_{\rm ch}$ and baryon chemical potential $\mu_{\rm B}$. A universal $T_{\rm ch}$ appears for all systems at high energies from e^+e^-, p-p and A+A. It is approximately equal to the QGP transition temperature predicted by lattice QCD calculations.

The center of mass energy for collisions of the heaviest ions at the LHC will exceed that available at RHIC by a factor of about 30. This opens up a new physics domain with exciting opportunities for seeking for QGP. The LHC/ALICE experiment will provide access to effectively all observable relevant for heavy ion physics at LHC energies, ranging from the low $p_{\rm T}$ region (>0.1 GeV/c) up to very high $p_{\rm T}$ of ≈100 GeV/c. To soft physics, we can get observables as yields of identified particles, correlations, event-by-event observable and flow.

References

1 Tannenbaum M J. arXiv: nucl-ex/0702028
2 WANG Ya-Ping, ZHOU Dai-Mei, HUANG Rui-Dian, CAI Xu. Chin. Phys. C (HEP & NP), 2008, **32**(4): 308
3 ZHOU Dai-Mei, WANG Ya-Ping, WEI Li-Hua, CAI Xu. Chin. Phys. C (HEP & NP), 2008, **32**(5): 400
4 CAI Xu, ZHOU Dai-Mei. HEP & NP, 2002, **26**(9): 971 (in Chinese)
5 Lacey R A. Nucl. Phys. A, 2006, **774**: 199
6 Schnedermann E, Heinz U W. Phys. Rev. C, 1994, **50**: 1675
7 van Leeuwen M et al. (NA49 Collaboration). Nucl. Phys. A, 2003, **715**: 161c
8 Barannikova O, WANG F et al. (STAR Collaboration). Nucl. Phys. A, 2003, **715** : 458c
9 Heinz U. arXiv: hep-ph/0407360
10 Burward-Hoy J M et al. (PHENIX Collaboration). Nucl. Phys. A, 2003, **715**: 498c
11 Ollitrault J Y. Phys. Rev. D, 1992, **46**: 229; Nucl. Phys. A, 1998, **638**: 195c
12 Heiselberg H, Levy A M. Phys. Rev. C, 1999, **59**: 2716
13 Voloshin S A, Poskanzer A M. Phys. Lett. B, 2000, **474**: 27
14 Sorge H. Phys. Rev. Lett., 1999, **82**: 2048
15 Acherman K H et al. (STAR Collabration). Phys. Rev. Lett., 2001, **86**: 402
16 Adams J et al. (STAR Collaboration). Phys. Rev. C, 2005, **72**: 014904
17 Adler C et al. (STAR Collaboration). Phys. Rev. Lett., 2003, **90**: 032301
18 Teaney D. Phys. Rev. C, 2003, **68**: 034913
19 Adare A et al. (PHENIX Coolaboration). nucl-ex/0608033
20 Issah M et al. (PHENIX Coolaboration). nucl-ex/0604011
21 Lacey R A, Taranenko A et al. (PHENIX Coolaboration). nucl-ex/0610029
22 Taranenko A et al. (PHENIX Coolaboration). J. Phys. G: Nucl. Part. Phys., 2007, **34**: S1069
23 Nouicer R. (PHOBOS Coolaboration). J. Phys. G: Nucl. Part. Phys., 2007, **34**: S887
24 Gustafsson H A et al. (Plastic Ball Collaboration). Phys. Rev. Lett., 1984, **53**: 544
25 Snellings R J M et al. Phys. Rev. Lett., 2000, **84**: 2803
26 Csernai L P, Roehrich D. Phys. Lett. B, 1999, **458**: 454
27 Brachmann J et al. Phys. Rev. C, 2000, **61**: 024909
28 Adams J et al. (STAR Collaboration). Phys. Rev. Lett., 2004, **92**: 062301
29 Alt C et al. (NA49 Collaboration). Phys. Rev. C, 2003, **68**: 034903
30 Kolb P F. Phys. Rev. C, 2003, **68**: 031902
31 Borghini N, Ollitrault T Y. Phys. Lett. B, 2006, **642**: 227
32 CHEN L W, Ko C M, LIN Z W. Phys. Rev. C, 2004, **69**: 031901; Kolb P F, CHEN L W, Greco V, Ko C M. Phys. Rev. C, 2004, **69**: 051901
33 BAI Y T. (STAR Collaboration). J. Phys. G: Nucl. Part. Phys., 2007, **34**: S903
34 Ullrich T S (STAR Collaboration). Nucl. Phys. A, 2003, **715**: 399
35 van Leeuwen M et al. (NA49 Collaboration). Nucl. Phys. A, 2003, **715**: 161c
36 Ulrich Heinz. arXiv: hep-ph/0407360
37 Hofman D J et al. (PHOBOS Collaboration). J. Phys. G: Nucl. Part. Phys., 2007, **34**: S217
38 Suire C et al. (STAR Collaboration). Nucl. Phys. A, 2003, **715**: 470c
39 Kolb P F, Rapp R. Phys. Rev. C, 2003, **67**: 044903
40 Huovinen P et al. Phys. Lett. B, 2001, **503**: 58
41 Rafelski J et al. Phys. Rev. Lett., 1982, **48**: 1066; Phys. Rev. Lett., 1986, **56**: 2334; Phys. Rep., 1986, **142**: 167
42 Andersen E et al. Phys. Lett. B, 1998, **433**: 209A
43 C Lamont M A (STAR Collaboration). J. Phys. G: Nucl. Part. Phys., 2006, **32**: S105
44 XU Zhangbu. (STAR Collaboration). arXiv: nucl-ex/0207019
45 Antinori F et al. (NA57 Collaboration). J. Phys. G: Nucl. Phys., 2006, **32**: 427
46 Redlich K, Tounsi A. Eur. Phys. J. C, 2002, **24**: 589
47 Becattini F et al. Phys. Rev. C, 2004, **69**: 024905
48 Adams J et al. (STAR Collaboration). Phys. Rev. Lett., 2004, **92**: 182301
49 Olga Barannikova (STAR Collaboration). arXiv: nucl-ex/0403014
50 Adcox K et al. (PHENIX Collaboration). Nucl. Phys. A, 2005, **757**: 184
51 Majumder A et al. J. Phys. Conf. Ser., 2005, **27**: 184
52 Van Buren G. (STAR Collaboration). Nucl. Phys. A, 2003, **715**: 129
53 Adler C et al. Phys. Rev. Lett., 2002, **89**: 092301
54 Gábor I Veres (PHOBOS Collaboration). J. Phys. G: Nucl. Part. Phys., 2007, **34**: S1103